Near–focus active optics: an inexpensive method to improve mm–wavelength radio telescopes

A. Greve[1], J.W.M. Baars[2,3]

[1] IRAM, 300 rue de la Piscine, 38406 St. Martin d'Hères, France
[2] Max Planck Institut für Radioastronomie, Auf dem Hügel 69, 53121 Bonn, Germany
[3] Submillimeter Telescope Observatory, University of Arizona, Tucson AZ 85721, USA

received date; accepted date

Abstract. The application of active and adaptive optics allows the construction of large diameter leight–weight *optical* telescopes, operating below the seeing limit of the atmosphere. Active wavefront correction in a Cassegrain/Gregory type *radio* telescope can be made with a deformable main reflector or deformable subreflector. Here we draw attention on the possibility of correction of spatially large–scale wavefront deformations with a small size corrector located near the focus of the telescope. As representative examples we calculate for the IRAM 30–m telescope the improvement obtained from the correction of (1) the systematic component in homology deformations, (2) the large–scale residual errors of a reflector adjustment, and (3) the beam degradation experienced in observations with a wobbling subreflector. The improvement in surface/wavefront precision obtained only from piston correction with a corrector of some 50 elements is of the order of 30 – 40 %.

We investigate in particular the systematic component of homology deformations, their representation by low order Zernike polynomials, and their elimination by near–focus correction. We study in detail the homology deformations of the IRAM 30–m reflector and the Effelsberg 100–m reflector.

Key words: radio telescopes – wavefront correction – homology – reflector surface errors – wobbling

1. Introduction

The spectacular progress in the construction of large diameter optical telescopes, and the success in the correction of atmospheric seeing at near–infrared and visible wavelengths, are primarily due to the development and application of active and adaptive optics (cf. Tyson 1991, Ryabova & Zakharenko 1992, Beckers 1993). In optical terminology, *active* optics is the correction of gravity, temperature, and wind induced large–scale and slowly varying deformations of the telescope's main mirror; *adaptive* optics is the correction of atmosphere induced fast deformations of the incident wavefront. The application of active optics allows the use of thin leight–weight monolithic mirrors and of segmented mirrors (see the telescopes of the VLT, ESO, and the Keck telescopes, USA); the application of adaptive optics allows the use of single telescopes and optical interferometers near the diffraction limit of the principal aperture. In radio astronomy, active wavefront correction is today obtained by application of homology (von Hoerner 1967) and deformation of the subreflector surface in a Cassegrain/Gregory system. The lack of detailed and fast imaging prevents the application of adaptive radio wavefront correction, although anomalous refraction may severely disturb the radio beam (Altenhoff et al. 1987, Downes & Altenhoff 1990).

In this paper we discuss for millimeter wavelength radio telescopes the possibility of *active wavefront correction near the focus* where the beam, and thus a corrector, is relatively small in diameter. The small size of the beam at this location allows only correction of spatially large–scale wavefront errors which, nonetheless, may contribute a substantial part of the total wavefront deformation. An active near–focus corrector, with a reasonably small number of elements ($\sim$ 50), should be relatively easy to build and to operate; it allows correction of wavefront errors introduced by the main reflector and the subreflector. To date, two experiments have demonstrated the feasibility of near–focus wavefront correction at millimeter wavelengths.

We summarize the methods of active radio wavefront correction either proposed or applied so far; then we present three numerical examples of the IRAM 30–m telescope which demonstrate the improvement that can be obtained from near–focus wavefront correction. The examples discuss (1) the correction of elevation–dependent residual systematic surface deformations of homologous reflectors; (2) the correction of large–scale main reflector adjustment errors; and (3) the correction of beam degradation experienced in observations with a wobbling subreflector. The emphasis of the discussion concentrates on the possibility to correct the systematic component of homology deformations; we analyze in detail the IRAM 30–m reflector and the Effelsberg 100–m reflector.

Send offprint requests to: A. Greve

2. Methods of active wavefront correction

Active wavefront correction can be made with the main reflector (I), for instance by modifying the position of panels in case they are supported by actuators; with the subreflector (II), by using a contoured or deformable surface; and with a contoured or deformable mirror near the focus (III), for instance located on the co–rotating mirror of a Nasmyth system (where field rotation does not occur) or a beam folding mirror of a Coudé system. This correction is achromatic, and does not affect the amplitude of the wavefront.
We do not consider lenses because of their chromatism and losses, and the difficulty in realizing a variable pathlength.

I. Correction using the main reflector

As a particular concept of mechanical construction, a homologous reflector (von Hoerner 1967) provides active wavefront correction by constraining the gravity induced deformations of the backstructure such that for all elevations the deformed reflector remains a paraboloid within the tolerance specification.

Several operating (sub–)millimeter wavelength telescopes have actuator supported panels (for instance JCMT, IRAM, SEST), however, these devices have not (yet) been used to actively shape the main reflector surface. The GBT 100–m telescope (USA, Vanden Bout 1991), presently under construction, will have actuator controlled panels to compensate gravity, temperature, and wind induced surface deformations. The 'instantaneous' data for correction are expected to be supplied from a laser ranging surface surveying system (Payne et al. 1992). The proposed 50–m millimeter wavelength telescope (LMT, USA) will have an active surface of hexagonal panels; computer simulations of the surface precision and beam shape obtained from active control on this telescope have been published by Cortes–Medellin & Goldsmith (1994).

II. Correction using the subreflector

There are two reported applications of a deformable subreflector; one for correction of elevation–dependent astigmatism of the Greenbank 43–m reflector (von Hoerner & Wong 1979), the other for correction of gravity induced deformations of the Haystack 37–m reflector (Antebi et al. 1994, Barvainis et al. 1993). A contoured, though not deformable subreflector is used on the Kitt Peak 12–m telescope (Mayer et al. 1994). The theory of a contoured subreflector for correction of main reflector deformations is published by von Hoerner (1976), Langley & Parker (1979), Milner & Bates (1980), and Lawson & Yen (1988).

Dependent on the diameter to wavelength ratio (d/λ) of the subreflector, geometric optics ray tracing or the Kirchhoff–Huygens–Silver formalism of diffraction can be used to derive the subreflector contour which compensates the main reflector surface deformation. In the application of ray tracing, the contour of the subreflector is derived from Snell's law and the condition that rays have equal path length and do not cross. Ray tracing is appropriate for a subreflector of large ratio d/λ and smooth surface gradients. Von Hoerner (1976) presents calculations for a correcting subreflector of size d/λ = 3.2 m/ 1.3 cm = 240, as used on the Greenbank 43–m telescope. In the application of the Kirchhoff–Huygens–Silver formalism of diffraction, the compensating contour is derived from the far field phase distribution of a spherical wave emanating from the focus and being scattered on the surface of the deformed subreflector. This theory was used by Langley & Parker (1979) to derive the contour of a subreflector of size d/λ = 15 cm/ 7.5 mm = 20. Similar cases are discussed by Rush (1963), Potter (1967), and Rush & Potter (1970).

III. Correction using an intermediate near–focus mirror

Active wavefront correction is possible near the focus, though only of large–scale deformations because of the small beam diameter at this position and the relatively large size corrector elements necessary to avoid additional diffraction. Contoured, though not deformable mirrors located near the focus were used on the Texas 5–m telescope (Mayer et al. 1991) and the IRAM 30–m telescope (Greve et al. 1994) for correction of wavefront deformations from the main reflector.
Wavefront correction near the focus can be made in case the phase distribution in the correction plane is similar to the deformed phase distribution of the aperture plane, in our case the main reflector or subreflector surface. Both planes must be located beyond the far–field distance z_{ff} of the feed which for the IRAM 30–m telescope is $z_{ff} = 2\ d^2/\lambda \approx 500\ \lambda$ for the applied feeds of aperture diameter $d \approx 10 - 15\ \lambda$. For λ = 3 mm, and shorter wavelengths, the co–rotating Nasmyth mirror at 3.5 m distance from the focus is in the far–field and thus a convenient place for a corrector, as verified in our experiment.

3. The systematic component of homology deformations

The application of homology minimizes gravitational deformations and allows the construction of large diameter, high precision, steerable radio telescopes for observations at centimeter, millimeter, and sub–millimeter wavelengths. The examples discussed here are the IRAM 30–m telescope (Baars et al. 1994) and the Effelsberg 100–m telescope (Hachenberg et al. 1976). Inspection of the surface error topographies calculated for homologous reflectors (cf. Hachenberg 1968, Mar & Liebowitz 1969), and of the telescopes mentioned above, shows that the elevation–dependent residual gravity deformations consist for one part of large–scale systematic deviations and for another part of small–scale random errors. While it is difficult to reduce the random errors, here we demonstrate that it is worthwhile to remove, at least partially, the component of systematic deformations.

In the concept of homology, the best–fit contour of the tiltable reflector remains at all elevation angles (ϵ) a paraboloid with tolerable surface deviations of rms (root mean square) value $\sigma(\epsilon)$. The panels of the reflector are adjusted to the specified surface contour at the elevation ϵ_0 ($\approx 45°$) around which most of the observations are made. This adjustment eliminates at ϵ_0 the residual gravity deformations such that for all reflector elements i (= 1,2, ..., K) the effective homology deformations are $\delta_{H,i}(\epsilon_0) = 0$, while otherwise in general $\delta_{H,i}(\epsilon) \neq 0$ for $\epsilon \neq \epsilon_0$. The rms–value σ_H of the homology deformations is

$$\sigma_H(\epsilon) = \sqrt{\sum_{i=1,K} \delta_{H,i}(\epsilon)^2/K}\ , \quad \sigma_H(\epsilon_0) = 0 \qquad (1)$$

and

$$\sigma_H(\epsilon)^2 = \sigma_H(0)^2[cos\epsilon - cos\epsilon_0]^2 + \sigma_H(90)^2[sin\epsilon - sin\epsilon_0]^2 \qquad (2)$$

with $\sigma_H(0)$ and $\sigma_H(90)$ the surface rms–values at horizon ($\epsilon = 0°$) and zenith position ($\epsilon = 90°$) (von Hoerner 1975).

The specified reflector contour at elevation ϵ_0 is realized only with the precision of the adjustment $\sigma_a(\epsilon_0)$ (rms–value). When tilted at elevation ϵ, the homology deformations superimpose so that the effective precision of the reflector is $\Sigma(\epsilon) = \sqrt{\sigma_a(\epsilon_0)^2 + \sigma_H(\epsilon)^2}$, where we assume that the homology deformations and adjustment errors are uncorrelated.

The large–scale component of the homology deformations $\delta_H(\epsilon,\rho,\theta)$ (of a circular reflector with normalized polar coordinates ρ [$0 \le \rho \le 1$] and θ [$0 \le \theta \le 2\pi$]) is conveniently expressed as a superposition of Zernike polynomials $Z_{nm}(\rho,\theta) = R_n(\rho)\cos(m\theta)$ and random residuals $\delta_{RAN}(\epsilon,\rho,\theta)$ such that

$$\delta_H(\epsilon,\rho,\theta) = \sum_{n,m} \alpha_{nm}(\epsilon) Z_{nm}(\rho,\theta) + \delta_{RAN}(\epsilon,\rho,\theta) \qquad (3)$$

The radial functions R_n are given by Born & Wolf (1980); the orders n,m used in this investigation are listed in Table 1. The coefficients α_{nm} of Eq.(3) can be uniquely determined from a least squares calculation (Wang & Silva 1980).

Table 1. Zernike Polynomials used in the Decomposition of Surface Deformations (Definition of the Index L).

L	1	2	3	4	5	6	7	8	9	10	11
n	0	2	4	6	1	3	5	7	2	4	6
m	0	0	0	0	1	1	1	1	2	2	2
L	12	13	14	15	16	17	18	19	20		
n	3	5	7	4	6	5	7	6	7		
m	3	3	3	4	4	5	5	6	7		

There are special designations for L = 3 (n=4,m=0): spherical aberration, L = 6 (n=3,m=1): coma, L = 9 (n=2,m=2): astigmatism.

We are only interested in large–scale wavefront deformations of low order n and m which represent areas of the reflector surface larger than panel dimensions and which can be smoothed with a small size near–focus corrector. Hence we restrict, somewhat arbitrarily, the decomposition of $\delta_H(\epsilon,\rho,\theta)$ to polynomials of the order $n \le N_0 = 7$ and $m \le M_0 = 7$. Figure 1 shows for the IRAM 30–m reflector and the Effelsberg 100–m reflector the coefficients $\alpha_{nm}(\epsilon)$ for $L \le 20$. It is evident from this figure that not all polynomials of the range (N_0, M_0) are important; we designate by $n^* \le N^*$ ($\le N_0$) and $m^* \le M^*$ ($\le M_0$) the sub–set of polynomials which gives a good representation of the systematic deformations. For the IRAM reflector we select 7 terms: $L^* = 3, 7, 9, 12, 13, 15, 17$; for the Effelsberg reflector we select 4 terms $L^* = 4, 5, 7, 8$. The systematic surface deformation δ_Z represented by these *leading* Zernike polynomials is

$$\delta_Z(\epsilon,\rho,\theta) = \sum_{n*,m*} \alpha_{nm}(\epsilon) Z_{nm}(\rho,\theta) \qquad (4)$$

Figure 2 illustrates this decomposition for the IRAM reflector. The figures indicated **H** show the homology deformations $\delta_H(\epsilon)$ predicted from the structural calculations. The figures indicated **Z** show the systematic deformations $\delta_Z(\epsilon)$ of the leading Zernike polynomials (N^*,M^*). The figures indicated **H − Z** show the homology deformations with the leading Zernike polynomial deformations being removed, leaving the random errors $\delta_{RAN}(\epsilon)$. A similar decomposition (not shown) is obtained for the Effelsberg reflector.

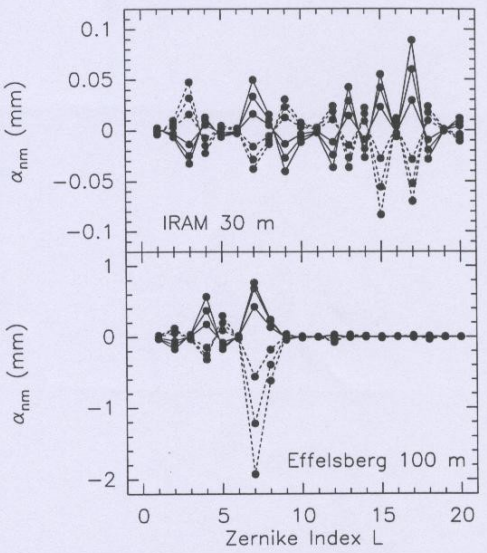

Fig. 1. Decomposition of homologous reflector deformations in Zernike polynomials (for the index L see Table 1). Coefficients α_{nm} for ϵ = 90°, 75°, 60°: solid lines, for ϵ = 30°, 15°, 0°: dashed lines. The reflectors are assumed to be perfectly adjusted at 45° elevation, thus $\alpha_{nm}(45°) = 0$.

4. Improvement from elimination of Zernike polynomial deformations

As evident from Fig. 2, the elimination of the low order Zernike polynomial deformations gives a surface with smaller and more randomly distributed errors (maps **H–Z**). We investigate the improvement from a calculation of the increase in reflector surface precision and the corresponding increase in aperture efficiency and smoothing of the gain–elevation dependence. For this we introduce the rms–value σ_{H-Z} of the residual surface errors of which the systematic deformations δ_Z are removed

$$\sigma_{H-Z}(\epsilon) = \sqrt{\sum_{i=1,K} [\delta_{H,i}(\epsilon) - \delta_{Z,i}(\epsilon)]^2 / K} \qquad (5)$$

Because the surface of the reflector is adjusted to the precision $\sigma_a(\epsilon_0)$, the realistic quantities to compare are the surface accuracies *without* correction

$$\Sigma_H(\epsilon) = \sqrt{\sigma_H(\epsilon)^2 + \sigma_a(\epsilon_0)^2} \qquad (6)$$

and *with* correction

$$\Sigma_{H-Z}(\epsilon) = \sqrt{\sigma_{H-Z}(\epsilon)^2 + \sigma_a(\epsilon_0)^2} \qquad (7)$$

For the IRAM reflector and the Effelsberg reflector we show in Fig. 3a the quantities σ_H, σ_{H-Z}, and Σ_H, Σ_{H-Z} for representative values $\sigma_a(\epsilon_0)$. The figure indicates a significant increase

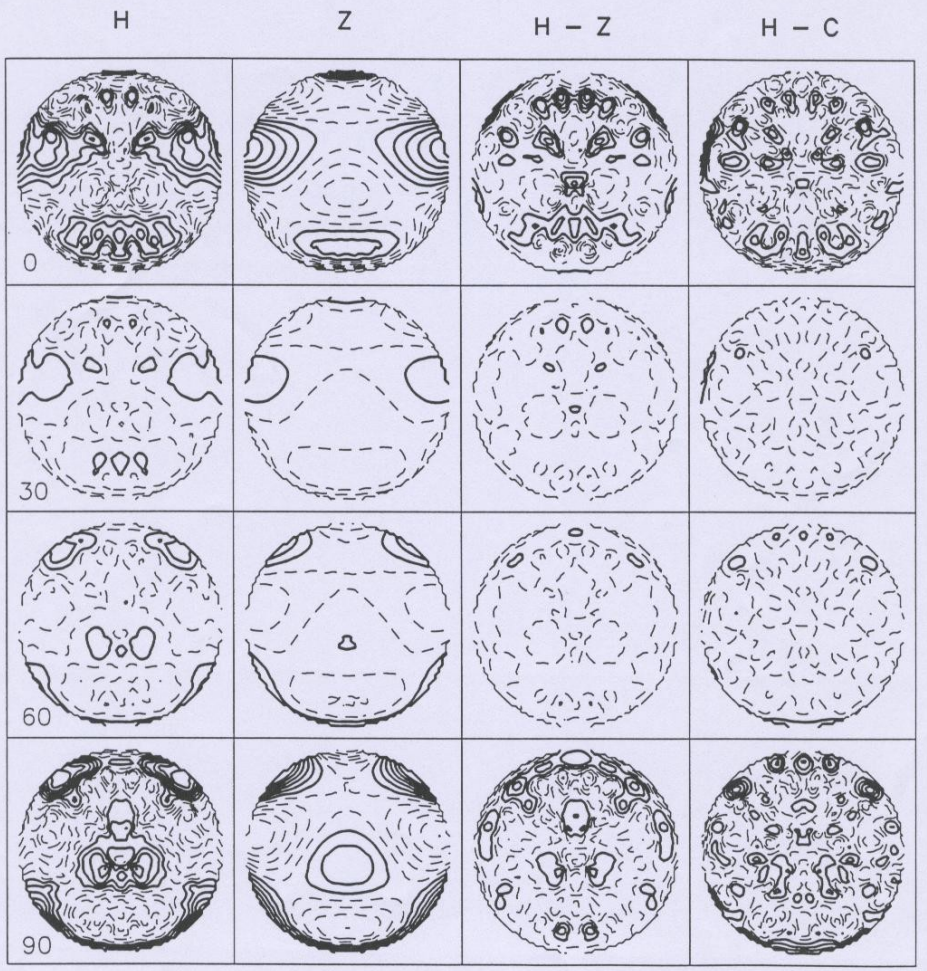

Fig. 2. IRAM 30–m reflector. **H**: predicted homology deformations (δ_H), **Z**: deformation of leading Zernike polynomials (δ_Z), **H–Z**: homology deformations minus leading Zernike polynomial deformations (δ_{H-Z}), **H–C**: homology deformations minus piston correction of the 52–element corrector shown in Fig. 4; calculated for the elevation $\epsilon = 0^0$, 30°, 60°, 90°. The reflector is assumed to be perfectly adjusted at $\epsilon_0 = 45°$. Contour levels: 0.02 mm.

of the reflector surface precision, worthwhile of correction, in particular when the adjustment precision does not dominate the reflector surface accuracy.
Following Ruze (1966), the aperture efficiency η_A of the reflector is

$$\eta_A(\epsilon) = \eta_0 \; exp(-[4\pi\sigma_{TP}(\epsilon)/\lambda]^2) \qquad (8)$$

with $\sigma_{TP}(\epsilon)$ the tapered–phase rms–value of the wavefront (Greve & Hooghoudt 1981), λ the wavelength of observation, and $\eta_0 = \eta_A(\lambda = \infty)$ = constant. For a steep reflector of focal ratio ~ 0.35 and illumination between $-$ 10 dB and $-$ 15 dB, we have $\sigma_{TP}(\epsilon) \approx 0.8\ \Sigma(\epsilon)$. In case of uncorrelated homology deformations and adjustment errors, the normalized gain–elevation dependence $g(\epsilon) = \eta(\epsilon)/\eta(\epsilon_0)$ of the wavefront *without* correction is

$$g_H(\epsilon) \approx exp(-[0.8\ 4\pi\sigma_H(\epsilon)/\lambda]^2) \qquad (9)$$

and *with* correction

$$g_{H-Z}(\epsilon) \approx exp(-[0.8\ 4\pi\sigma_{H-Z}(\epsilon)/\lambda]^2) \qquad (10)$$

Figure 3b shows the predictions of the gain–elevation dependence $g_H(\epsilon)$ and $g_{H-Z}(\epsilon)$, using the values of Fig. 3a. Evidently, the correction of the large–scale deformations produces a significant decrease of the gain–elevation dependence.
The large–scale deformations are not strictly statistical errors. However, we have shown earlier (Baars 1973, Greve 1980) that Ruze's formula applied to systematic wavefront deformations gives often a good prediction of the main beam degradation. For the present cases we have verified our analysis by diffraction calculations which give results in agreement with those presented here.

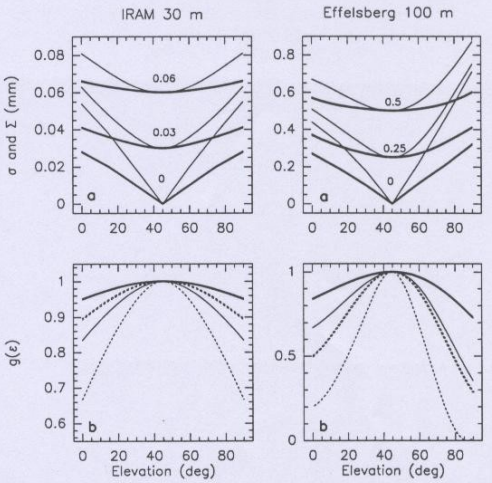

Fig. 3. a) Increase in reflector surface precision by elimination of the leading Zernike polynomial deformations. Not corrected (σ_H, Σ_H): thin lines, corrected (σ_{H-Z}, Σ_{H-Z}): thick lines. The inserted values indicate the adjustment accuracy $\sigma_a(\epsilon_0)$ (mm). **b)** Predicted gain–elevation dependence g_H *without* (thin lines) and g_{H-Z} *with* (thick lines) correction of leading Zernike polynomial deformations. IRAM 30–m reflector for λ = 1.3 mm (230 GHz): ———, for λ = 0.86 mm (350 GHz): – – –. Effelsberg 100–m reflector for λ = 7 mm (43 GHz): ——— , for λ = 3 mm (86 GHz, full illumination): – – –.

5. Near–focus active wavefront correction

We discuss now three numerical examples for the IRAM 30–m telescope to demonstrate the improvement which can be obtained from near–focus correction. The selected corrector, shown in Fig. 4, has 52 square–shaped elements which allow, for simplicity, only piston correction. We ignore edge diffraction at the elements since the actual corrector will have a continuous surface. The corrector is located on the co–rotating Nasmyth mirror.

5.1. Active homology

From the homology calculations we derive for each corrector element the average deformation of the projected reflector area (Fig. 4), and we impose that the corresponding wavefront deformation is eliminated by a compensating piston displacement of the corresponding corrector element. In normal astronomical observations the piston displacement ($\lesssim$ 0.15 mm) is a slowly varying function of elevation. The topography of the predicted correction (**H** $-$ **C**), displayed in Fig. 2, shows little difference with the topography (**H** $-$ **Z**) in which the leading Zernike polynomial deformations are removed. The residual surface rms–value σ_{H-C} obtained from piston correction is given in Table 2 together with the rms–value σ_{H-Z} for correction of the leading Zernike polynomial deformations. We find $\sigma_{H-C} \approx \sigma_{H-Z}$ for n $\gtrsim$ 50, hence a corrector of some 50 elements operating in piston mode eliminates the major contribution of

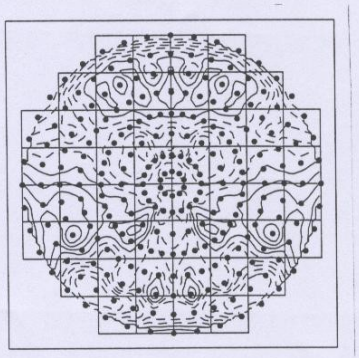

Fig. 4. Aperture plane projection of the 52 square–shape element piston mode corrector. The dots show the positions for which homology calculations are available (IRAM 30–m telescope). Four adjacent dots outline a panel frame, each supporting 2 panels. The contour levels show the homology deformations at horizon.

the large–scale deformation. For the 52–element corrector the corresponding increase in reflector precision and smoothing of the gain–elevation dependence are similar to those shown in Fig. 3a,b. When located on the co–rotating Nasmyth mirror, the diameter of the corrector is $\sim$ 35 cm. For $\lambda = 1.3$ mm (230 GHz) the corresponding ratio d/λ of the corrector elements is given in Table 2. A similar corrector for main reflector astigmatism, with elements of size d/λ = 30 mm/ 1.3 mm = 23, performed well in an experiment on the 30–m telescope (Greve et al. 1994). We are therefore confident that a 52–element corrector placed on the Nasmyth mirror will correct equally well the large–scale component of the homology deformations.

Table 2. IRAM 30–m telescope. Predicted Surface/Wavefront Improvement by Piston Correction using an n–Element Corrector [Values in mm].

	Elevation	0°/90° a)	30°/60° a)	d/λ b)
No correction	σ_H	0.055	0.020	
Zernike Polyn.	σ_{H-Z}	0.028	0.010	
Piston n = 32	σ_{H-C}	0.040	0.014	45
Piston n = 52 c)	σ_{H-C}	0.034	0.012	34
Piston n = 86	σ_{H-C}	0.031	0.011	27

a) identical values for ϵ and $90° - \epsilon$. For $\epsilon = 45°$: $\sigma = 0$.
b) for $\lambda = 1.3$ mm (230 GHz) and the corrector located on the Nasmyth mirror.
c) the corrector is shown in Fig. 4.

5.2. Active reflector surface adjustment

The adjustment of large main reflector surfaces is extremely labour consuming, unless the reflector panels are supported by motorized actuators. A typical case is the 30–m telescope where panel adjustments can only be made by hand. It therefore seems worthwhile to consider also for this case wavefront correction through elimination of large–scale adjustment errors using a near–focus active corrector.

For this telescope we present one example of residual adjustment errors. Figure 5 shows the surface error topography determined October 1993 from holography measurements at $\epsilon = 43°$ elevation using the geostationary satellite ITALSAT at 39 GHz (D. Morris, IRAM). At the outer panel rings the surface shows a large–scale deviation resembling that of an incomplete annular zone. The application of the 52–element piston corrector reduces the surface rms–value from $\sigma_a = 0.120$ mm to $\sigma_a = 0.078$ mm; the corresponding phase–tapered rms–values $\sigma_{TP} \approx 0.096$ mm and $\sigma_{TP} \approx 0.064$ mm would give an improvement of the aperture efficiency of $\eta_A(0.064)/\eta_A(0.096) \approx 1.62$ at $\lambda = 1.3$ mm. The corresponding smoothing of the surface error topography is shown in Fig. 5.

5.3. Active wobbling

At (sub–)millimeter wavelengths the strong and rapidly changing emission/absorption of the Earth's atmosphere swamps weak cosmic signals, unless differential observing procedures are applied. A frequently used method of sky subtraction is based on on–source off–source measurements with the beam displaced on the sky by wobbling of the telescope's subreflector. The wobbling is made with a frequency of $\sim$ 1 – 10 Hz and a focal plane beam throw of 30 – 300″. In order to observe

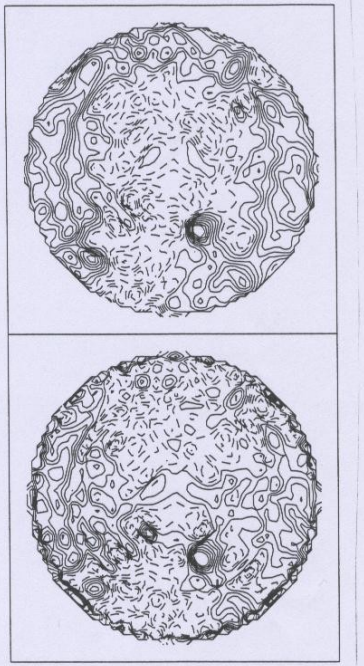

Fig. 5. IRAM 30–m reflector surface error topography at elevation $\epsilon = 43°$; October 1993 (later re–adjusted). Upper panel: measured topography showing the actual deviations, lower panel: predicted error topography after piston correction with the 52–element corrector shown in Fig. 4. Contour levels: 0.025 mm.

under symmetric conditions, the on–source and off–source positions are located at equal and opposite distances off–axis. The subreflector of a Cassegrain system wobbles either around its vertex or a location between its vertex and the main reflector focus. The tilt ($\Delta\alpha$) and associated shift (Δx) of the subreflector introduces a coma–like wavefront deformation with corresponding beam degradation, in particular noticeable as reduction of the beam peak power (cf. van der Stadt 1984).

Figure 6 shows for the 30–m telescope the reduction in peak power at 2 mm (150 GHz) and 1.3 mm (230 GHz) wavelength introduced by wobbling of the subreflector. The observational data are extracted from calibrated scans across Mars with the subreflector tilted such that the focal plane displacement of the source was 60″ and 120″, respectively. An active near–focus corrector, which follows the wobble frequency (here 1 – 2 Hz) and corrects the wavefront according to the applied wobble throw, will restore to large extent the beam profile and the loss in power. We illustrate the improvement expected from the 52–element piston corrector.

Following Ruze(1969) and Zarghamee & Antebi (1985), the tilt $\Delta\alpha$ and the associated shift Δx of the subreflector introduces a displacement of the beam in the focal plane $\Delta\beta = \Delta\beta_\alpha - \Delta\beta_x$, where

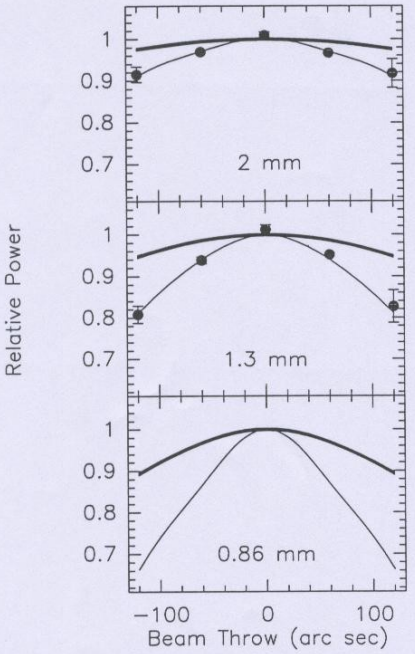

Fig. 6. IRAM 30–m telescope loss in peak power in observations with the wobbling subreflector. Dots: measurements; thin lines: loss in peak power calculated for the wavefront deformation of Eq.(13–14); thick lines: restauration of peak power by application of the 52–element piston corrector of Fig. 4. [There are no observations at 0.86 mm].

$$\Delta\beta_\alpha = (c-a)[K(n)+K(N)]\Delta\alpha/f \tag{11}$$

$$\Delta\beta_x = [K(n)-K(N)/M]\Delta x/f \tag{12}$$

with $\Delta x = p(c-a)\Delta\alpha$, (c – a) the distance between the subreflector vertex and the primary focus, and p ($0 \le p \le 1$) the fractional distance of the wobble axis from the subreflector vertex. For the 30–m telescope (c – a) = 690 mm and p = 0.56. The tilt and shift cause a large–scale coma–like wavefront deformation $\varphi(\rho,\theta) = \varphi_\alpha(\rho,\theta) - \varphi_x(\rho,\theta)$ where

$$\varphi_\alpha = k(c-a)[E(\rho,n)+ME(\rho,N)]\Delta\alpha\ sin\theta \tag{13}$$

$$\varphi_x = kp(c-a)[E(\rho,n)-E(\rho,N)]\Delta\ \alpha sin\theta \tag{14}$$

with $k = 2\pi/\lambda$, M = 27.8 the magnification of the 30–m telescope, n = f/D = 0.35 the focal ratio of the main reflector, and N = Mn = 9.7 the effective focal ratio of the system. (ρ, θ) are the normalized polar coordinates of the aperture. The function E(ρ,m) is

$$E(\rho,m) = (8m\rho)/[(4m)^2+\rho^2] \tag{15}$$

The beam deviation factors K(m) are taken from figure 3 of Zarghamee & Antebi's publication, i.e. K(n=0.35) = 0.75 and K(N=9.7) = 1.0 for a taper $f(\rho) = 1 - \alpha\rho^2$ with $\alpha = 0.75$.

As evident from Fig. 7, the piston correction of the 52–element corrector predicts a convincing restauration of the beam profile. The predicted recovery of the beam peak power is shown in Fig. 6.

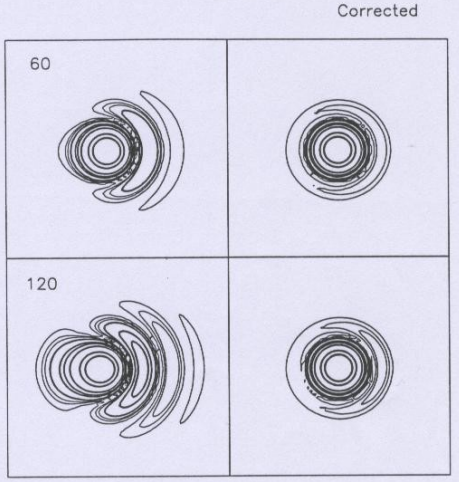

Fig. 7. Beam profiles at 230 GHz showing the performance of the 52–element piston corrector (Fig. 5) for a beam throw of 60″ and 120″. Countor levels of thin lines: – 30, – 25, –23 dB, of heavy lines: – 20, – 15, – 13, – 10, – 5, – 3 dB.

6. Conclusion

So far, the feasibility and efficiency of active radio wavefront correction has been demonstrated in only relatively few applications, using the subreflector surface as active element. Here we have illustrated for a millimeter wavelength telescope that the correction of large–scale wavefront deformations can be made near the focus with a corrector of relatively small size and a reasonably small number of elements ($\sim$ 50). The reported experiments at millimeter wavelengths (Mayer et al. 1991, Greve et al. 1994) have clearly demonstrated the success of near–focus wavefront correction.

We have discussed three examples of near–focus correction of large–scale wavefront deformations. Although these examples are specific of the IRAM 30–m telescope, they may stimulate further experiments and the application of (piston mode) correctors on other telescopes.

The discussion of this paper does not proclaim the construction of cheap radio telescopes to be corrected later by active optics. On the contrary, the discussion intends to demonstrate a possibility to improve operating telescopes, or to correct telescopes with accidental wavefront deformations.

Acknowledgements: The homology calculations of the Effelsberg 100–m telescope and of the IRAM 30–m telescope were made by ARGE KRUPP(now VERTEX Antennentechnik GmbH)–MAN, Germany. D. Morris (IRAM France) kindly provided the holography measurements of Figure 5. S. Navarro and B. LeFloch (IRAM – Granada) helped with some calculations. Ruze's (1969) notes were brought to my attention by R. Predmore (FCRAO).

References

Altenhoff J.W., Baars J.W.M., Downes D., Wink J.E. 1987, AA 184, 381
Antebi J., Zarghamee M.S., Kan F.W., Hartwell H., Salah J.E., Milner S.M. 1994, IEEE Ant. Propag. Magazine 36, 19
Baars J.W.M. 1973, IEEE Trans. Ant. Propag. AP–21, 461
Baars J.W.M., Greve A., Hein H., Morris D., Peñalver J., Thum C. 1994, Proc. IEEE 82, 687
Barvainis R., Ball J.A., Ingalls R.P., Salah J.E. 1993, PASP 105, 1334
Beckers J.W. 1993, ARA&A 31, 13
Born M., Wolf E. 1980, *Principles of Optics*, Pergamon Press, Oxford
Cortes–Medellin G., Goldsmith P.F. 1994, IEEE Trans. Ant. Propag. AP–42, 176
Downes D., Altenhoff J.W. 1990, in *Radio Astronomical Seeing*, ed. J.W. Baldwin and Wang Shouguan, URSI–IAU Symp. Bejing, Intern. Academic Press, p. 31
Greve A. 1980, Appl. Optics 19, 2948
Greve A., Hooghoudt B.G. 1981, AA 93, 76
Greve A., LeFloch B., Morris D., Hein H., Navarro S. 1994, IEEE Trans. Ant. Propag. AP–42, 1345
Hachenberg O. 1968, *Studien zur Konstruktion des 100–m Teleskops*, Dümmlerbuch 702, Dümmler Verlag, Bonn
Hachenberg O., Wielebinski R., Grahl B.H. 1976, Proc. IEEE 61, 1288
Langley R.J., Parker E.A. 1979, IEEE Trans. Ant. Propag. AP–27, 527
Lawson P.R., Yen J.L. 1988, IEEE Trans. Ant. Propag. AP–36, 1343
Mar J.W., Liebowitz H. (ed.) 1969, *Structural Technology for Large Radio and Radar Telescope Systems*, MIT Press, Cambridge, MA.
Mayer C.E., Davis J.H., Foltz H.D. 1991, IEEE Trans. Ant. Propag. AP–39, 309
Mayer C.E., Emerson D.T., Davis J.H. 1994, Proc. IEEE 82, 756
Milner M.O., Bates R.H.T. 1980, Proc. Instr. Electr. Eng. 127, 277
Payne J.M., Parker D., Bradley R.F. 1992, Rev. Sci. Instrum. 63, 3311
Potter P.D. 1967, IEEE Trans. Ant. Propag. AP–15, 727
Rush W.V.T. 1963, IEEE Trans. Ant. Propag. AP–11, 414
Rush W.V.T., Potter P.D. 1970, *Analysis of Reflector Antennas*, Academic Press, New York – London
Ruze J. 1966, Proc. IEEE 54, 633
Ruze J. 1969, *Small displacements in parabolic reflectors*, MIT Lincoln Lab., Lexington Mass., USA
Ryabova N.V., Zakharenkov V.F. 1992, Sov. J. Opt. Techn. 59, 320
Tyson R.K. 1991, *Principles of Adaptive Optics*, Academic Press Inc., Boston – San Diego – New York
Vanden Bout P.A. 1991, Adv. Space Reas. 11, 387
van der Stadt H. 1984, IEEE Trans. Ant. Propag. AP–32, 1128
von Hoerner S. 1967, AJ 72, 35
von Hoerner S. 1975, IEEE Trans. Ant. Propag. AP–23, 689
von Hoerner S. 1976, IEEE Trans. Ant. Propag. AP–24, 336
von Hoerner S., Wong, W–Y. 1979, IEEE Trans. Ant. Propag. AP–27, 720
Wang J.Y., Silva D.E. 1980, Appl. Optics 19, 1510
Zarghamee M.S., Antebi J. 1985, IEEE Trans. Ant. Propag. AP–33, 828

This article was processed by the author using Springer-Verlag LaTeX A&A style file 1990.